USING SCALE TO OPTIMIZE THE WASTE-TO-ENERGY POTENTIAL OF APPLIED SMOULDERING SYSTEMS

Tarek L. Rashwan [a], José L. Torero [b], Jason I. Gerhard [a]*

[a] Department of Civil and Environmental Engineering, The University of Western Ontario, London, Ontario N6A 5B9, Canada

[b] Department of Civil, Environmental and Geomatic Engineering, University College London, London, WC1E 6BT, UK

* Corresponding author at: Department of Civil and Environmental Engineering, The University of Western Ontario, Spencer Engineering Building, Rm. 3029, London, Ontario N6A 5B9, Canada. Tel.: +1 (519) 661 4154; fax: +1 (519) 661 3942. E-mail address: jgerhard@uwo.ca (J. I. Gerhard).

One file containing supplementary material is available.

Abstract: Smouldering combustion has been demonstrated to be a highly energy efficient approach towards waste-to-energy. The benefits of smouldering are principally due to the matching of energy generation and transfer time scales as well as its low quenching temperature (<400°C). This enables effective energy extraction of problematic wastes (e.g., because of low-volatility or high-moisture content). As the engineering applications of smouldering combustion expand, there is a growing interest in designing systems to best house a propagating smouldering reaction. Through a series of experiments, this work quantifies the path of heat transfer that determines how heat lost at the perimeter of the reactor affects the relatively thin reaction zone Thermocouples were placed throughout radial and axial coordinates and integrated to estimate the net stored energy throughout the column volume with time. The impact of heat losses was normalized as the system energy efficiency, by dividing the net stored energy by the energy added into the column for ignition and released from smouldering. The results revealed that the system energy efficiency increased from 65 ± 3% to 86 ± 5% with column radius increasing from 0.080 m to 0.300 m, respectively. As a result, scenarios that were not self-sustaining in the thin column were demonstrated to be self-sustaining in the wider column. Thus, increased system energy efficiency increased the robustness of the reaction to quenching. Altogether, this work underscores the importance of scale as a crucial design parameter enabling a smouldering system to be used as an effective waste-to-energy approach.

Keywords: Smoldering combustion; Energy balance; Heat losses; Waste-to-Energy; Porous media; Process scale-up.

Symbols and Nomenclature

Abbreviations

BSS	Borderline-self-sustaining
CEMS	Continuous emissions monitoring system
FID	Flame ionization detector
GAC	Granular activated carbon
DF	Dilution factor
DRUM	Oil-drum sized column
LAB	Laboratory column
MAD	Median absolute deviation
NSS	Non-self-sustaining
MC	Wet basis moisture content
R	Robust experimental conditions
SS	Self-sustaining
TC	Thermocouple
W	Weak experimental conditions
WC	Wood chips

Latin Letters

A	Cross sectional area, m^2
C_p	Specific heat capacity, J kg^{-1} K^{-1}
dm/dt	Mass loss rate, kg s^{-1}
E	Energy, J
$\dot{E}$	Energy rate, J s^{-1}
fr_{CO}	Fraction of C oxidized to CO
L	System length, m
M	Molar mass, kg mol^{-1}
$\dot{M}''$	Molar flux, mol m^{-2} s^{-1}
m/m	Mass fraction
$\dot{m}$	Mass flow rate, kg s^{-1}
R	System radius, m
t_{ig}	Ignition time, s
t_f	Final time, s
T_{peak}	Maximum temperature, K
T_{amb}	Initial ambient temperature, K
v_{oxid}	Smouldering front velocity, m s^{-1}
$\dot{V}$	Volumetric flow rate, m^3 s^{-1}
X	Molar fraction

Greek Symbols

ΔH	Heat of smouldering, MJ kg^{-1}
Δt	Time between measurements, s
ϕ	Porosity

ρ	Density, kg m^{-3}
τ	Characteristic time, s

Subscripts

amb	Ambient
$down$	Downstream
eff	Effective
f	Final
i	Initial/entering
in	Into control volume
ig	Ignition
j	Radial position from centre
J	Radial position nearest to the wall
$loss$	Lost from control volume
net	Net stored
$oxid$	Oxidation
out	Out of control volume
pyr	Pyrolysis
s	Sand

1. Introduction

1.1. Applied Smouldering Combustion

Applications of smouldering combustion are solving a wide range of engineering challenges. Applied smouldering systems represent a simple, economical, and robust thermal conversion option in many contexts, including soil remediation [1-3], biomass energy conversion [4, 5], wastewater sludge treatment [6, 7], resource recovery [8, 9], and sanitation in the developing world [10, 11]. Thus, smouldering is emerging as a viable waste-to-energy option. Most of these applications require the design and construction of engineered smouldering systems (e.g., batch or continuous reactors). The scale of the reactor is intimately related to the waste-to-energy process, with some systems favouring small reactors [8, 11] while other larger systems [3, 12]. Thus, scale is a key variable defining the potential of smouldering as a waste-to-energy treatment. Meanwhile, most smouldering research - central to elucidating the underlying principles and parameter sensitivities of the technology - exists only at the laboratory (bench) scale. As a result, there is limited understanding of the effects of scale on smouldering behaviour, and this knowledge gap impairs the link between laboratory research and technology applications, as well as limits the predictive capacity current numerical models (e.g., [13-15]).

The operating principle of smouldering is heterogeneous, flameless combustion resulting from gaseous oxygen reacting with a condensed phase fuel comprising, or embedded within, a porous medium [16, 17]. In most contexts, smouldering is limited by the transport of oxygen to the surface of the reacting fuel [16, 18, 19]. A common example is glowing red charcoal in a traditional barbeque. As is recognized in barbeque design, the rate and

direction of air flow through the porous bed has a strong impact on the reaction. Moreover, as seen in barbeques, smouldering will propagate as a reaction wave through the bed until the fuel is exhausted or the air flow is eliminated. There is a wide range of fuels that smoulder, from natural materials such as peat [20], coal [21], and forest litter [22] to anthropogenic materials like polyurethane foam [23], oil-soaked insulation [24], and coal tar-contaminated soil [18, 25]. In uncontrolled smouldering scenarios, such as underground coal seam fires, smouldering proceeds in a runaway manner since the air flow cannot be eliminated, fuel load is in excess, and the system geometry is uncontrolled [21, 26]. In applied engineering scenarios, air flow is strictly managed, and fuel load and system geometry are carefully controlled to effectively destroy wastes and capture the released energy [8, 10, 18].

In most incinerators (e.g., fluidized bed), energy is delivered very quickly by the combustion reaction and thereby drives all other processes. Therefore, heat transfer processes can be simplified, but efficient use of the energy released is difficult. In contrast, a smouldering system is comprised of multiple *zones,* each characterized by different heat and mass transfer processes and chemical reactions [27], where no single process is dominant over the others. Consequently, heat transfer processes are complex but efficiency is potentially very high. In the *reaction zone,* including the smouldering front itself, competing pyrolysis and oxidation reactions govern the fuel conversion into, primarily, CO_2, CO, H_2O and heat [16]. In the *inert heating zone,* ahead of the smouldering front, the untreated fuel will undergo heat absorption (known as “preheating”) and drying. The *cooling zone* behind the smouldering front is also reaction-free where

hot porous material experiences heat dissipation. This set of coupled, interdependent zones propagate and vary in thickness and intensity throughout space and time. Thus, smouldering is a complex and dynamic thermal system, the fundamentals of which continue to be studied primarily in laboratory and theoretical research.

Smouldering as an applied waste-to-energy approach has some significant advantages over other thermal processes. As indicated above, smouldering has the potential of being an extremely energy efficient form of combustion, which allows for utilizing a wide array of combustible materials for effective energy recovery [8, 10, 18]. One reason for this is that the rates of fuel conversion and heat transfer are all driven by the porous medium and therefore have compatible characteristic time scales [10, 18]. A second reason is that the porous medium acts as a heat storage reservoir. The fuels in engineered smouldering systems are typically embedded in an inert porous medium, e.g., hydrocarbons in soil [28, 29], sludges or digestates in sand [7, 30, 31], and human faeces in zirconium oxide beads [11], which can store and recycle energy like flaming porous burners [32-34]. Finally, quenching temperatures for smouldering reactions are generally lower than 400°C [8, 30, 35], which enables the reduction of heat losses and propagation of the reaction with much lower effective energy generation.

If the airflow feeding the reaction is driven in the same direction as the smouldering front propagation, forward heat transfer from the cooling of the burnt region and the reaction zones is deposited in the inert heating zone [18, 36]. This efficient convective recycling of heat allows the treatment of wastes that are otherwise problematic for incinerators, such as those with low-volatility (e.g., tank bottom oil sludge) or high moisture content

(e.g., wastewater sludge) [8, 10, 18]. Currently, nearly every incineration technology uses flaming-based reactors [37-39], but for all problematic wastes it is necessary to either pre-process the waste (e.g., moisture removal, chemical treatment) or add supplemental fuel. In these cases it has been shown that these wastes are better handled in smouldering-based reactors [3, 5, 8, 10, 12, 29, 31, 40-42].

As a result, smouldering is self-sustaining under a wide range of conditions. Self-sustaining means that, after an initial small and local input of energy, the process will continue without external energy input indefinitely as long as sufficient fuel and air are present [16]. This is commonly observed after igniting charcoal in a barbeque. The underlying causes are positive energy balances both locally (at the reaction front) and globally (across the fuel bed), where the rate of heat generated reaches thermal equilibrium with the heat lost (e.g., to endothermic processes and to the external environment) at temperatures above quenching [16, 19, 43]. The self-sustaining nature of smouldering is what makes natural smouldering problems so intractable, such as peat forest and underground coal fires [21, 22, 26], and what makes applied smouldering waste-to-energy systems so green and sustainable [8, 10, 18, 25].

Due to these benefits, applied smouldering has been recently upscaled into a commercial technology. A pilot smouldering reactor demonstrated the ex situ treatment of coal-tar contaminated soil [44], which was similar in size as another smouldering reactor studied for deriving liquid fuel from waste tires [9]. Following [44], a modular, scalable, batch treatment system was developed for contaminated soils and organic sludges [3, 12, 45]. It has been applied in numerous cases, including in Southeast Asia for treating crude oil

lagoon sludge [3, 12] and applied in China for oil sludge mixed with contaminated soil [25]. In addition, another pilot smouldering reactor was developed that represented a 300-fold scale up of a typical laboratory column [25]. In all of these cases, it has been assumed that large scale smouldering systems behave similarly to laboratory systems, although almost no research exists on this topic.

Significant research – all at the laboratory scale – has explored how to maximize the envelope of self-sustaining behaviour in applied smouldering, including identifying and extending the quenching limits [13, 29, 42-44, 46, 47], optimizing the fuel/inert ratio [30, 35, 48-52], examining inert-free systems [5, 31, 53], and considering supplemental, low-volatility fuels for high-volatility wastes [54]. In all of these cases, the focus – whether explicitly acknowledged or not – was shifting the energy balance in the smouldering system to more positive values [13, 18, 43]. Though there are many inputs to resolve in a comprehensive system energy balance (e.g., energy for ignition, emissions treatment, compressed air), a key aspect of the energy balance is radial heat losses to the external environment. Given that the reaction front is very thin and that the effective thermal conductivity of the porous medium is low in applied smouldering systems [18, 43, 46, 55], radial heat losses have not been considered relevant to the smouldering stability, therefore this aspect has received little attention. Therefore, the link between system scale losses and smouldering stability has never been directly studied in applied smouldering systems.

Though heat transfer near the reactions closely match the heat generation time scales, heat transfer at the system scale is often much slower than smouldering propagation [18].

Therefore, the cooling zone temperatures are unsteady in most applied smouldering systems and the link between system scale losses and improved smouldering performance is not simple. Consequently, heat losses as a function of scale has never been quantified in applied smouldering systems (see an expanded discussion on this topic in the Supplementary Materials, Section S9). Furthermore, this problem is not easily rectified using existing data sets, since smouldering applications are not adequately instrumented, and no methodology exists to quantify system heat losses or energy efficiency.

1.2. The Energy Balance in Applied Smouldering Systems

Zanoni et al. provides insight into how heat losses affect smouldering propagation by developing a global energy balance around a one-dimensional smouldering system [13, 43]:

$$\dot{E}_{net} = \dot{E}_{in} + \dot{E}_{oxid} - \dot{E}_{pyr} - \dot{E}_{loss} - \dot{E}_{out} \quad (1)$$

where $\dot{E}_{in}$ is the rate energy is added from the igniter, $\dot{E}_{oxid}$ is the rate energy is added by exothermic oxidation, $\dot{E}_{pyr}$ is the rate energy is removed by endothermic pyrolysis, $\dot{E}_{loss}$ is the rate energy is removed by radial heat losses, $\dot{E}_{out}$ is the rate energy is lost due to convection at the system boundary, and $\dot{E}_{net}$ is the net rate of energy accumulation. At self-sustaining conditions away from the inlet and outlet boundaries $\dot{E}_{in}$ = $\dot{E}_{out}$ = 0; moreover, $\dot{E}_{pyr}$ has been shown to be negligible in many applied smouldering conditions [18, 43]. Therefore, $\dot{E}_{net}$ is primarily governed by $\dot{E}_{oxid}$ and $\dot{E}_{loss}$, and the balance

between them will dictate whether a smouldering system is self-sustaining ($\dot{E}_{net} \geq 0$), or trending towards extinction ($\dot{E}_{net} < 0$). Whether the smouldering reaction exists or not depends on the local energy balance at the reaction zone. If the conditions are such that the Damköhler number exceeds the critical value, then smouldering persists; otherwise, extinction will occur [74-76]. However, integrating Eq. (1) over the system (i.e., reactor bed and time), can provide measure of the robustness of the smouldering system [43]. Positive $\dot{E}_{net}$ indicates the smouldering system is increasing robustness, as the accumulating stored energy acts as a buffer against extinction [43]. At sufficiently late times with enough energy accumulated, modest changes in heat losses do not significantly affect smouldering characteristics [14, 43, 46, 55]. However, if this buffer against extinction is relatively small, but the Damköhler number remains above the critical value, weak smouldering occurs. This happens, for example, due to low oxygen flux or low fuel concentration [13, 30, 35, 43, 46, 66, 74, 77-79]. Under such conditions, slight changes in $\dot{E}_{loss}$, can strongly affect weak smouldering characteristics, dropping peak temperatures and propagation velocities [66]. Though weakened smouldering may persist, if $\dot{E}_{net}$ becomes negative for a sufficiently long time the Damköhler number will fall below the critical value and the system will trend to extinction [13, 43]. Altogether, numerical models [14, 43] and experiments [55] agree that 30-50% % of the energy generated from laboratory applied smouldering systems escape as heat losses. However, no quantification exists of how this fraction may decrease with increasing system scale, nor are there clear demonstrations of the expected increase in robustness.

To address the major gap between applied smouldering research and technology applications, this work quantifies the influence of scale on the system energy efficiency and demonstrates its implications on the smouldering reaction stability. The fraction of energy lost radially to the environment was determined for smouldering experiments using columns at a variety of diameters. The experiments spanned the spectrum from robust smouldering to weak smouldering to extinction conditions. The experiments were instrumented with radial and axial thermocouples and mass loss and emission products were measured. A new methodology was developed to permit global energy balances that quantified energy efficiency. Moreover, a rigorous global mass balance was employed on carbon to validate the reaction stoichiometry that was only assumed in previous work. This work provides the first quantification of the reduced heat losses, and therefore increased robustness, of self-sustaining smouldering systems as scale increases. Altogether, this work underscores the importance of scale as a crucial design parameter in optimizing an applied smouldering system and provides a valuable framework to estimate heat losses and energy efficiency at any scale.

2. Methodology

2.1. Experimental Equipment and Setup

All experiments followed established methods [29, 30, 35, 42] slightly adapted to use a convective ignition method in the laboratory column (LAB) and the oil-drum sized column (DRUM), illustrated in Fig. 1. Granular activated carbon (GAC, at least 90% particles larger than 80 mesh, DARCO® 12X40, Cabot Corp.) was used as a model fuel for this study because: 1) simple oxidation chemistry, 2) lack of pyrolysis reactions, 3) ease of mixing and experimental preparation, and 4) there is an emerging, practical interest in smouldering spent GAC from adsorption treatment [80]. GAC is similar to the charcoal used as a model fuel in [55], which reported the same benefits and simplified chemistry that was followed here. Proximate analysis indicated the GAC wet basis moisture content (MC) was 3.2% (ASTM-D2867-17), volatile matter content was 3.2% (ASTM-D5832-98), ash content was 2.2% (ASTM-D2866-11), and fixed carbon content was 91.4% (calculated by the difference). The GAC higher heating value was measured as 30.9 MJ kg^{-1} (IKA C 200 bomb calorimeter), which normalized to the combustible fraction (i.e., the sum of the volatile matter and fixed carbon) is 32.7 MJ kg^{-1} and compares well to the theoretical value for pure carbon, 32.8 MJ kg^{-1} [81] (see additional discussion on GAC characterization in the Supplementary Materials, Section S1).

Table 1 presents the experimental conditions, illustrating that the variables adjusted were column diameter, fuel concentration, and applied air flux. The experimental conditions reflect both common values used in applied smouldering research (e.g., [30, 54, 65, 80, 82]) and application (e.g., [3, 28, 45]). The GAC was mechanically mixed with coarse

grain sand (1.180 ≤ mean grain diameter ≤ 2.000 mm, porosity (ϕ) = 0.37, bulk density ($[1-\phi]\rho_s$) = 1670 kg m^{-3}, MC between 0.04% and 0.4%, Number 12, Bell & Mackenzie) to desired fuel concentrations (example photo in the Supplementary Materials, Fig. S2). The GAC and sand exhibited similar grain sizes and were mixed and packed into the columns with sufficient care that heterogeneity was not apparent in any data acquired. All DRUM experiments had a 0.054 to 0.098 m clean sand cap on top of the fuel bed to lower the exiting air temperature when the smouldering front approached the top of the column (for safety purposes). Experiments DRUM R1, R2, and W2 also included a loosely packed, 0.027 to 0.030 m layer of wood chips (WC; see Supplementary Materials, Section S5 for details) on top of a 0.010 to 0.040 m bottom layer of clean sand to facilitate ignition at lower temperatures. Smouldering the GAC led to a small drop in the fuel bed height (3% to 5%) in all experiments; the three experiments with an ignition WC layer incurred an additional height drop equal to the WC layer thickness.

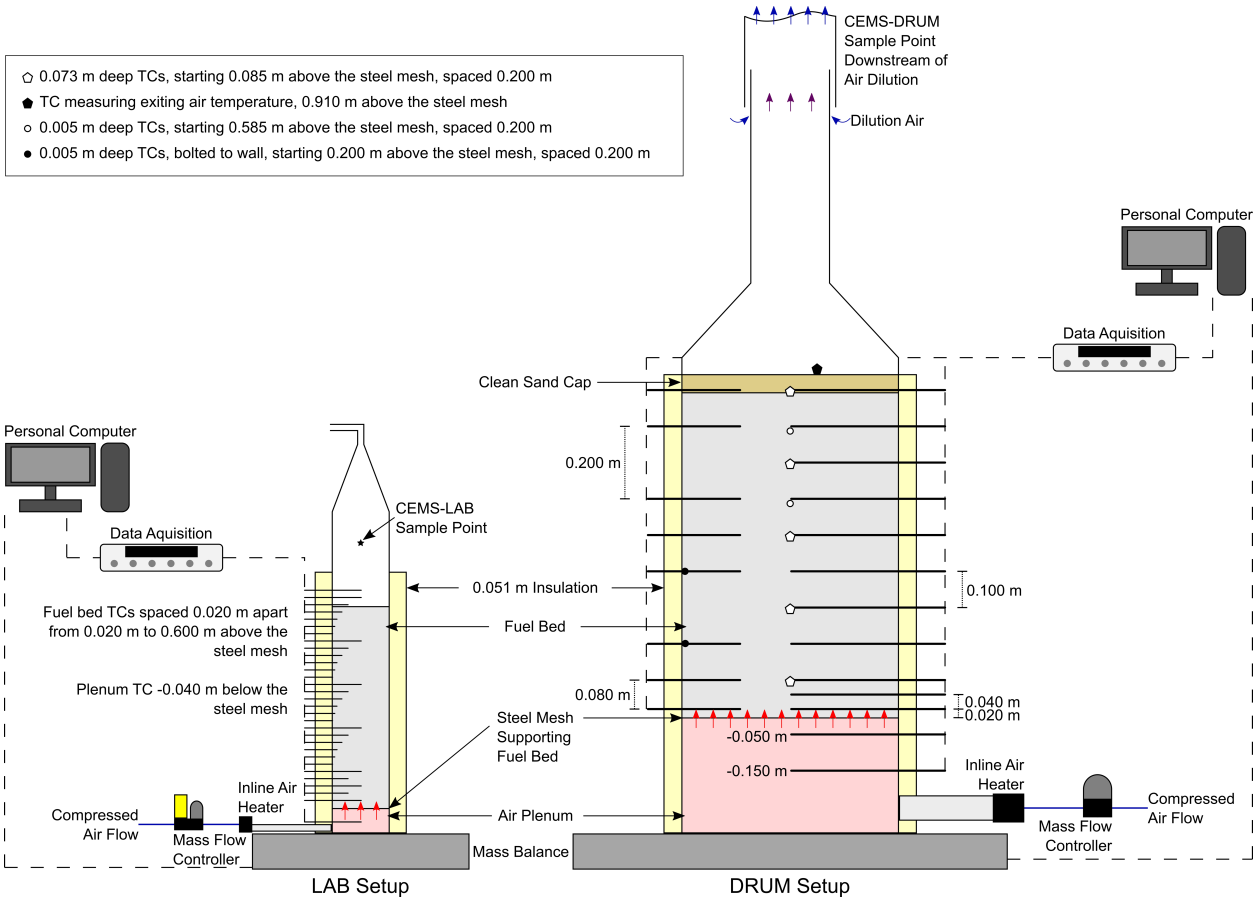

Fig. 1. Illustration of the LAB and DRUM experimental setups. LAB thermocouples (TCs) are placed 0.080 m, 0.043 m, 0.026 m, 0.012 m, 0.006 m, and 0.000 m deep from the column wall into the column centre. DRUM TCs placed 0.300 m, 0.165 m, 0.073 m, and 0.005 m deep from the column wall into the column centre.

Table 1. Experimental Conditions and Key Smouldering Front Results

Experimental Conditions				Smouldering Front Results			
Experiment	GAC/sand (g_{GAC} kg_s^{-1}) LAB ± 0.3% DRUM ± 2%	Darcy air flux[1] (cm s^{-1}) LAB ± 3% DRUM ± 2%	Initial fuel bed height (m) ± 0.003 m	Borderline-/Non-/Self-sustaining? (BSS/NSS/SS)	Mean centreline propagation velocity (cm min^{-1}) LAB ± 4% DRUM ± 10%	Mean centreline peak temperature (°C) LAB ± 1% DRUM ± 4%	Mean $\frac{CO(\%)}{CO(\%)+CO_2(\%)}$[2] LAB ± 10% DRUM ± 2%
Robust							
DRUM R0	20.0	5.0	0.813	SS	0.46	804	-[a]
[3] DRUM R1	20.0	7.5	0.868	SS	0.47	765	-[a]
[3] DRUM R2	23.3	5.0	0.865	SS	0.44	834	-[a]
[4] LAB R1	20.0	7.5	0.568	SS	0.61	766	0.27
[4] LAB R2	23.3	5.0	0.560	SS	0.49	874	0.27
Weak							
[5] DRUM W1	10.0	5.0	0.719	BSS	0.19	601	0.26
[6] DRUM W2	20.0	1.0	0.874	SS	0.16	782	0.29
[7] LAB W1	10.0	5.0	0.253	NSS	-	-	-
[7] LAB W2	20.0	1.0	0.262	NSS	-	-	-
[7] LAB W3	15.0	5.0	0.277	SS	0.33	661	0.18
[4,7] LAB W4	20.0	2.0	0.255	SS	0.24	678	0.13

Experimental Conditions' errors represent conservative estimates of equipment error.

Smouldering Front Results' errors encompass a conservative estimate of experimental variability as they represent the normalized standard deviations from three DRUM and LAB repeat experiments from smouldering wastewater sewage sludge, a highly variable fuel [30]. These errors align well with similar experimental studies [30, 54, 65, 80, 82].

[1] At standard temperature and pressure (21.1°C at 1 atm).

[2] The percentages represent vol.% values.

[3] Used a thin bottom layer of wood chips for ignition and recycled sand.

[4] Mass balance results were spurious because the instrumentation caused small erratic physical vibrations.

[5] Used a thin bottom layer of wood chips below a bottom 0.128 m layer of 20.0 g_{GAC} kg_s^{-1} layer for ignition.

[6] The fr_{CO} averaging began after 194 min from turning off the heater because of persistent initial effects (see Fig. S3(a)) and used a manual rotameter to control low air flow (0-0.010 m^3 s^{-1}, King Instrument Company).

[7] Used a less instrumented experimental setup using conductive ignition described in [30].

[a] CO measurement throughout propagation exceeded CEMS-DRUM calibration range, which was 0-0.3%.

The LAB and DRUM columns were similarly constructed with stainless-steel and inner radii of 0.080 m and 0.300 m, respectively, and wrapped in 0.051 m thick insulation for safety purposes (ASTM C518 R-Value = 8.7 at 24°C, MinWool®, Johns Manville [LAB]; ASTM C518 R-Value = 9.6 at 24°C, FyreWrap® Elite® Blanket, Unifrax [DRUM]). Both setups used similar mass flux controllers (FMA5400/5500 Series, Omega Ltd. [LAB]; 8290B045PDB67 ASCO Numatics [DRUM]), inline air heaters for convective ignition (F074719 2 kW SureHeat® JET [LAB], F074736 36 kW SureHeat® MAX [DRUM], Osram Sylvania), and mass balances (KCC150 [LAB], KD1500 [DRUM], Mettler Toledo). Thermocouples (Type K, 0.0032 m diameter Omega Ltd. [LAB], 0.0064 m diameter Kelvin Technologies [DRUM]) were placed in various radial and axial positions (Fig. 1). All emissions sampling locations are noted in Fig. 1. Continuous emissions monitoring systems (CEMS) were used in the LAB (CEMS-LAB for O_2, CO_2, and CO, MGA3000C, ADC) and DRUM experiments (CEMS-DRUM, custom assembly with a URAS for CH_4, CO_2, CO, and a FID for unburned hydrocarbons, ABB Ltd.). The CEMS-DRUM and mass balances logged directly to a personal computer with equipment specific software every 5 and 2 seconds, respectively. All other instruments were connected to a data logger (Multifunction Switch/Measure Unit 34980A, Agilent Technologies) and personal computer that logged every 2 and 3 seconds for the LAB and DRUM experiments, respectively.

2.2. Experimental Procedure

Ignition was achieved via injecting hot air (300-400°C in the DRUM and 400-500°C in the LAB, the maximum air temperatures using the respective setups) into the column plenum

until the thermocouples (TCs) located 0.1 m above the plenum reached peak smouldering temperatures, 700-900°C. The convective heater was then turned off and ambient temperature air was injected at the desired air flux to sustain propagation. Experiments LAB W1, W2, W3, and W4 used a conductive ignition method and less instrumented setup as detailed in [30]. Though there were differences in the ignition procedure, all experiments showed signs of strong ignition in the temperature histories (i.e., very high peak temperatures near the heater) and upon excavation (i.e., no fuel remaining around the heater). Moreover, the ignition method is not expected to affect the results presented in this work, which focuses on front propagation away from the boundaries. The smouldering front characteristics reported in Table 1 were averaged after turning off the heater and fixing the ambient air flux until the front reached the last centre TC, at least 0.01 m from the end of the fuel bed. The mean centreline propagation velocity, centreline peak temperature, and fr_{CO} were all relatively steady during this time, and the most data scatter was observed in the weak experiments (see Supplementary Materials, Fig. S3). The propagation velocities were calculated from observing the front arrival at successive thermocouples, following the method in [41].

The experiments in Table 1 are separated into “robust” and “weak” experimental conditions and, within these categories, robust or weak self-sustaining (SS), borderline-self-sustaining (BSS), and non-self-sustaining (NSS) by following the criteria in [30] and by considering mass loss behaviour. The measurements in Fig. 2 shows the overall normalized mass removed from the reactors over time and provides insight into smouldering robustness. Figure 2 shows the spectrum of mass loss behaviour in these

experiments from NSS to weak BSS to robust SS smouldering, where the shallower slopes indicate a weak or weakening reaction, and the end point of each curve near Non-Dimensional Time = 1 indicates the effectiveness of the treatment process (i.e., the fraction of fuel removed from the system by smouldering).

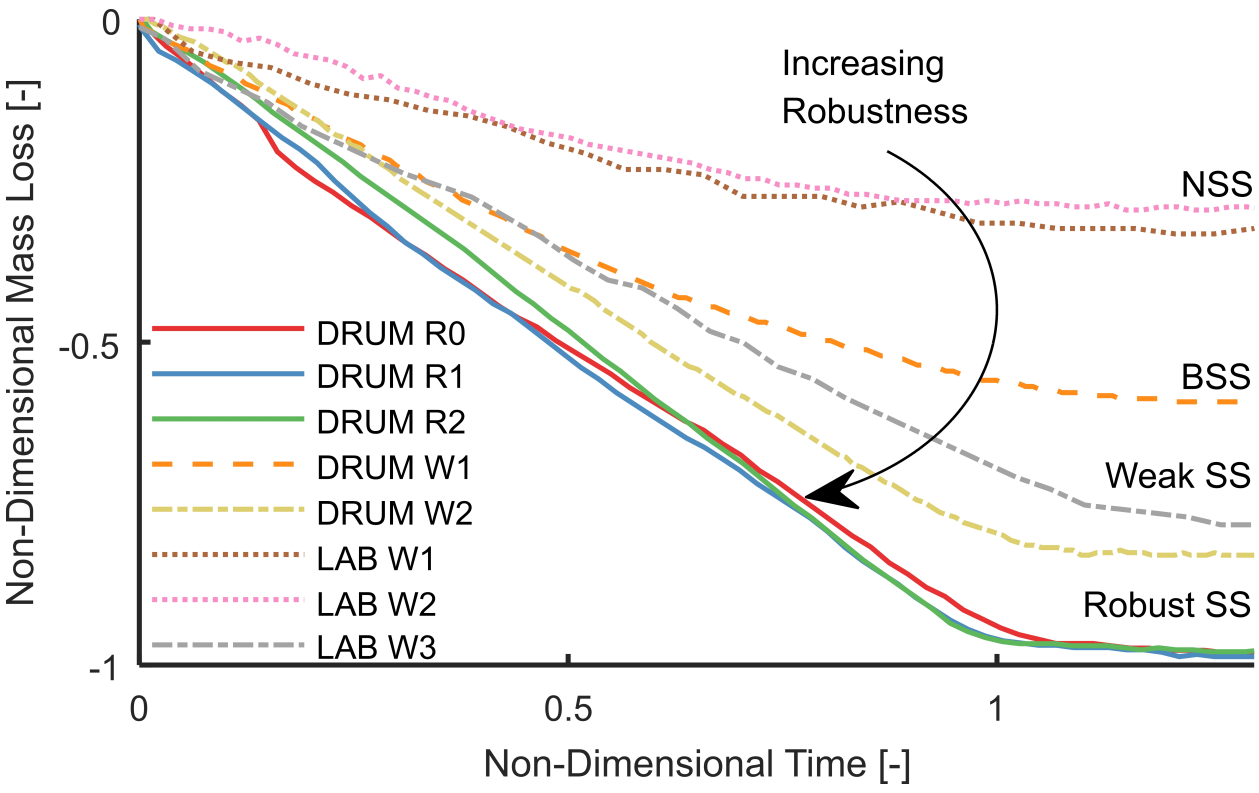

Fig. 2. Non-dimensional mass loss profiles from all DRUM and weak LAB experiments (where the mass was normalized to the total smoulderable mass in each experiment). The graphs plot every 100th data point for clarity and are bounded by the end of ignition (Non-Dimensional Time = 0) and the end of propagation (Non-Dimensional Time = 1). The non-self-sustaining (NSS, LAB W1 and W2), borderline-self-sustaining (BSS, DRUM W2), weak self-sustaining (Weak SS, DRUM W2 and LAB W3), and robust self-sustaining (Robust SS, DRUM R0, R1, and R2) experiments are noted. The methods for making the mass and time non-dimensional are detailed in the Supplementary Materials, Section S2.

2.3. Global Energy Balance

A global energy balance was conducted on the experiments. Equation (1) was employed assuming $\dot{E}_{out}$ = 0, since the time of specific interest was before the smouldering front reached the top of the fuel bed at the end of propagation (t_f), and neglecting $\dot{E}_{pyr}$, which has been shown to be minor relative to the other terms in other applied smouldering systems [43] and neglected here because of the simple GAC degradation (see discussion in Section 2.1 and the Supplementary Materials Section S1). However, this is not valid in all cases as pyrolysis will be more relevant for other fuels under various smouldering conditions [18]. Here, the chemistry is only approximated, and some pyrolysis reactions evolving CO/CO_2 may be embedded within the estimated $\dot{E}_{oxid}$ term. Nevertheless, the following analysis will be structured as if the net heat released from smouldering is from a an effective oxidation term, which aligns with previous smouldering research using similar fuels [46, 55, 83, 84]. The fundamental chemistry steps within smouldering systems, even simple systems using pure carbon, GAC, or charcoal, presents an opportunity for future research [18]. Isolating the unknown term in Eq. (1) on the left:

$$\dot{E}_{loss} = \dot{E}_{in} + \dot{E}_{oxid} - \dot{E}_{net} \quad for\ 0 < t < t_f \tag{2}$$

Integrating each of these terms in time from time zero (turning on the heater) solves E_{loss} during propagation:

$$E_{loss}(t) = E_{in}(t) + E_{oxid}(t) - E_{net}(t) \tag{3}$$

$$for\ 0 < t < t_f$$

The method for calculating each of these are discussed in turn, since this represents the first global energy balance presented for an experimental smouldering system.

The total energy accumulated from the heater at every measurement time, $E_{in}(t + \Delta t)$, was estimated by:

$$E_{in}(t + \Delta t) = E_{in}(t) + \int_{T_{amb}}^{T_{air}(t)} \dot{m}_{air}(t) C_{p_{air}}(T_{air}) dT \Delta t \qquad (4)$$

$$for\ 0 < t$$

where the air mass flow $(\dot{m}_{air})$ was known, the ambient temperature (T_{amb}) was taken as the background plenum temperature, and the injected air temperature (T_{air}) was taken as the plenum temperatures nearest to the fuel bed (0.04 m and 0.05 m below the LAB and DRUM fuel bed, respectively). The timestep (Δt) was the time between temperature measurements, and a quadratic approximation for the heat capacity of air was used $\left(C_{p_{air}}(T_{air}) = -3x10^{-5}T_{air}^2 + 0.2261T_{air} + 940.35\right)$ [85, 86].

The total energy generated from smouldering, $E_{oxid}(t)$, was estimated from the GAC ignition time $\left(t_{ig}\right)$ to t_f as:

$$E_{oxid}(t + \Delta t) = E_{oxid}(t) + v_{oxid}(t)(1 - \phi)\rho_s \frac{m_{GAC}}{m_s} A \Delta H_{oxid} \Delta t \qquad (5)$$

$$for\ t_{ig} \leq t < t_f$$

The mean smoulder velocity (v_{oxid}) and GAC bulk density ($[1-\phi]\rho_s\, m_{GAC}/m_s$), which assumes the GAC occupied a fraction of the sand pore space, were specific to each experiment. The radial extent covered by TCs was used to calculate the column cross-sectional area (A), i.e., the full 0.080 m radius in the LAB analysis and 0.295 m of the 0.300 m radius in the DRUM analysis (Fig. 1). Equation 5 estimates the cumulative energy released over time based on the extent of propagation. Furthermore, v_{oxid} was observed to be relatively steady after turning off the heater in each robust experiment when the air flux was fixed (see Supplementary Materials, Fig. S3(b)). Additional discussion on steady smouldering and the methods used to identify t_{ig} and t_f are detailed in the Supplementary Materials, Section S3.

The heat of smouldering (ΔH_{oxid}) was estimated as if the GAC was pure carbon, where ΔH_{oxid} varied with the fraction of C oxidized to CO (fr_{CO}) [46, 55, 83, 84]:

$$C + \left(\frac{fr_{CO}}{2} + [1 - fr_{CO}]\right) O_2 \rightarrow fr_{CO} CO + (1 - fr_{CO}) CO_2 \qquad (6)$$

fr_{CO} has a strong impact on ΔH_{oxid}, i.e., ΔH_{oxid} = 110.5 to 393.5 kJ molc^{-1} for fr_{CO} = 1 to 0, respectively [46, 81]. A fr_{CO} = 0.27 was determined from experiments LAB R1 and R2 (Table 1). Like v_{oxid}, fr_{CO} was relatively steady throughout each experiment (see Supplementary Materials, Figs. S3(a-b)). This provides a GAC ΔH_{oxid} = 24.9 MJ kg^{-1}, adjusted to account for the inert ash and water vaporization in GAC. ΔH_{oxid} was assumed constant between all robust experiments.

To confirm Eq. (6) using fr_{CO} = 0.27 was accurate, it was used in mass balance calculations to predict the concentrations of CO, CO_2, and O_2 in the emissions from robust experiments and compared to measurements. For experiments LAB R1 and R2, in which mass loss data was not available, the rate of C oxidation was approximated from each experiment's v_{oxid}. For experiments DRUM R0, R1, and R2, the rate of C oxidation was additionally approximated from each experiment's mass loss rate profile. In all cases, the measured O_2, CO, and CO_2 concentrations were accurately calculated. Details are included in the Supplementary Materials, Section S4 (with the key results in Fig. S5). This confirmed that it is appropriate to assume the entire combustible fraction of GAC oxidized from C to CO and CO_2 using fr_{CO} = 0.27.

As a wood chip (WC) layer was used to ignite DRUM R1 and R2, an additional energy generation term $\left(E_{oxid_{WC,eff}}\right)$ was used to estimate the energy released from smouldering the WC layer, which was similar to Eq. (5) but used the WC properties. The details on estimating and implementing $E_{oxid_{WC,eff}}$ are included in the Supplementary Materials, Section S5.

The net stored energy, E_{net}, was estimated by integrating the change in thermal energy in the sand. The energy stored in the air-filled porosity was neglected and the measured temperatures were assumed to represent the sand temperatures since $(1-\phi)\rho_s C_{p_s} \gg \phi C_{p_g}\rho_g$ [65]. E_{net} was estimated from temperatures measured throughout the systems' volume at every measurement time with the embedded TCs:

$$E_{net}(t) = \iiint_{V} \int_{T_{amb}}^{T_s(l,r,t)} (1-\phi)\rho_s C_{p_s}(T_s) dT dV \quad (7)$$

$$for\ 0 < t$$

The temperature was assumed to vary linearly between the measurement points. The linear expression for sand heat capacity, $\left(C_{p_s}(T) = 1.75T_s + 340.32\right)$ and sand bulk density ($[1-\phi]\rho_s =$ 1670 kg m^{-3}) from [86] was used, as the same coarse grain sand was used in all experiments here. The integration in Eq. (7) was completed in two steps at every temperature measurement time and built upon the E_{net} calculation method in [86]. Further details on how this was implemented is included in the Supplementary Materials, Section S6.

The system energy efficiency as a function of time was calculated by:

$$System\ Energy\ Efficiency(t) = E_{net}(t)/[E_{in}(t) + E_{oxid}(t)] \quad (8)$$

As the bottom and top sections of the columns were the least instrumented, system energy efficiencies were only estimated over height intervals where they could be calculated reliably, heuristically determined as the times when the front propagated from 0.30 to 0.50 m and 0.30 to 0.70 m in the LAB and DRUM experiments, respectively.

3. Results and Discussion

3.1. The Effects of Heat Losses on Robust Smouldering Systems

Figure 3 visualizes the temperatures at various times from experiments LAB R2 and DRUM R2, which were representative of the patterns in all robust experiments.

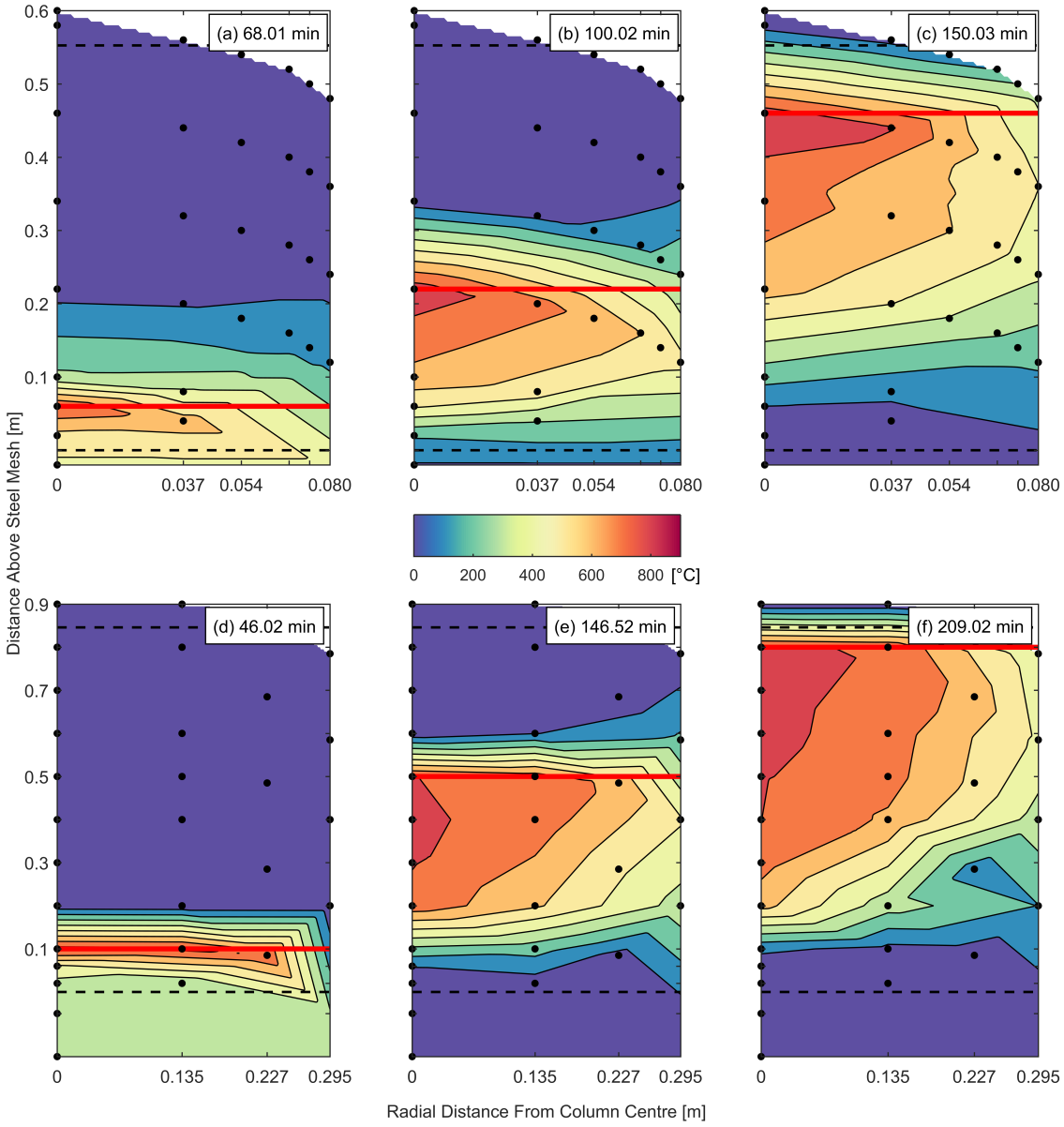

Fig. 3. (a-c) LAB R2 and (d-f) DRUM R2 colour contour maps show the temperature distribution across the column radius and axis at specific times. The black circles mark the thermocouple locations and the black dashed lines bound the fuel bed region upon excavation. The red lines show the approximate smouldering front positions: (a, d) just after ignition, (b, e) part-way up the column, and (c, f) near the end of the column. The plenum air temperatures were assumed uniform over the column radius.

Figure 3 reveals the temperature gradients from the column centre to the wall, driven by radial heat losses. Much of the energy released from smouldering accumulated in the cooling zone behind the smouldering front, which is characteristic for forward smouldering that is reaction leading [36]. Because nearly all heat losses from the DRUM and LAB experiments were drawn from this cooling zone [43], the temperatures needed to be well resolved in this region to conduct a global energy balance. Figure 3 shows that by spacing TCs across radial and axial locations, the temperature distribution was sufficiently captured to estimate E_{net} profiles.

Other details are revealed from Fig. 3. For example, the temperatures ahead of the smouldering fronts show the areas near the walls heated faster than the centre (most clearly seen above the red lines in Figs. 3(b) and 3(e)). This aligns with other studies that have shown the smouldering front is not typically flat but often curved across the radius in the direction of propagation because the cooler air temperatures near the column wall facilitates enhanced axial convective heat transfer [14, 46, 55]. Furthermore, though the TCs capture the temperature profiles behind the smouldering front well, they do not resolve the sharp temperature change in the combustion zones ahead of the smouldering front (just above the red lines in Fig. 3). Others have shown that applied smouldering in similar configurations facilitates a thin combustion zone (~0.01 m, where temperatures vary from T_{ig} to T_{peak}) [14, 43, 46, 55]. As the vertical spacing was larger here (see Fig. 1), these steep gradients were not well resolved. Because only a thin region in the system is impacted by these measurement errors, the key trends from the global energy balance are largely unaffected.

Figure 4 presents the E_{net} profiles for experiments LAB R2 and DRUM R2 (plots for the other robust experiments are included in the Supplementary Materials, Fig. S7). It reveals how the net stored energy grew in both experiments from when the smouldering front ignited until it reached the top of the fuel bed, reaching peaks of approximately 7 and 200 MJ in LAB R2 and DRUM R2, respectively. Beyond these times, E_{net} decreased reflecting the column cooling due to radial and convective losses. The jaggedness in the E_{net} curves are an artefact of the TC spacing in the experiments. Numerical modelling of E_{net} calculations as a function of TC spacing revealed that: (1) the true E_{net} does increase monotonically as expected, (2) the E_{net} estimate becomes more smooth as vertical discretization increases, (3) achieving a monotonic result would require experiments with TC spacing < 0.01 m, and (4) the intersections in E_{net} and $E_{in} + E_{oxid}$ are artefacts, with sufficient TC spacing, $E_{in} + E_{oxid}$ is always greater than E_{net} (see Supplementary Materials, Section S7, and Fig S6). An approximation of the true E_{net} function is illustrated in Fig. 4 for qualitative interpretation.

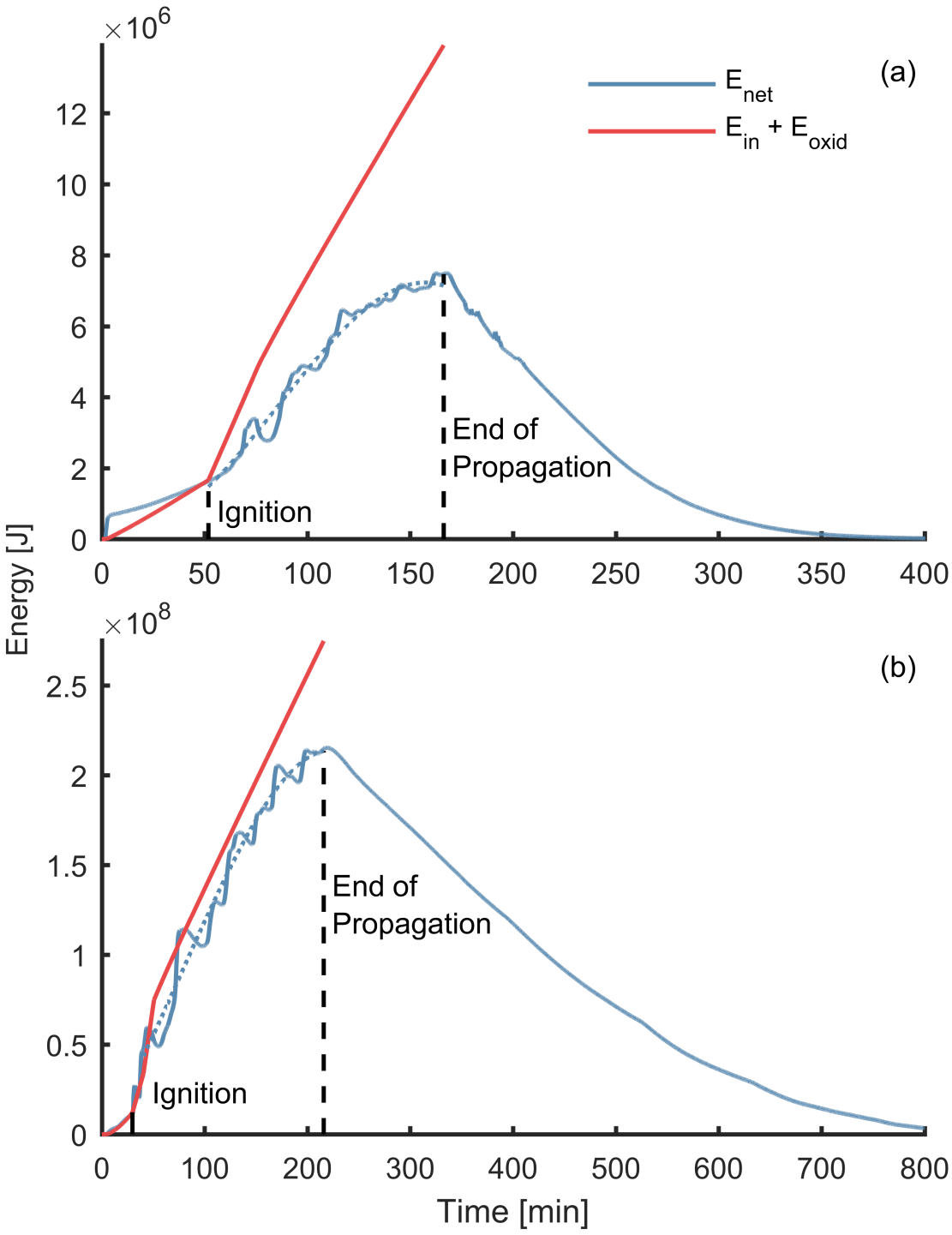

Fig. 4. The E_{net} and $E_{in} + E_{oxid}$ profiles from (a) LAB R2 and (b) DRUM R2. Ignition and end of propagation are noted on both figures and the dotted blue lines are fitted curves to illustrate the approximate correct E_{net} profiles without the false oscillations.

The sum of $E_{in}(t) + E_{oxid}(t)$ are also plotted in Fig. 4, with the first term mainly contributing the energy prior to ignition and the latter contributing thereafter. If the columns were perfectly insulated, all of the energy added would remain stored in the hot sand until convective losses began near the end of smouldering [13, 43], and $E_{net}(t)$ would equal $E_{in}(t) + E_{oxid}(t)$. Thus, the differences between $E_{in}(t) + E_{oxid}(t)$ and $E_{net}(t)$ in Fig. 4 reveal $E_{loss}(t)$ (see Eq. (3)). The figure clearly demonstrates that radial losses are proportionally less in DRUM R2 than in LAB R2.

Figure 5 shows the influence of scale on smouldering performance by plotting the system energy efficiencies, $E_{net}(t)/[E_{in}(t) + E_{oxid}(t)]$, for all robust experiments when the smoulder front travelled approximately 0.3 to 0.5 m. It reveals that the median system energy efficiency was 65 ± 3% for the LAB experiments and 86 ± 5% for the DRUM experiments when the front travelled ~0.4 m; the uncertainty values indicate the median absolute deviations (see the Supplementary Materials for the grouped results, Fig. S9). A two-sample Kolmogorov-Smirnov test showed the DRUM experiments system energy efficiencies are larger than those of the LAB at the 0.01% significance level [87].

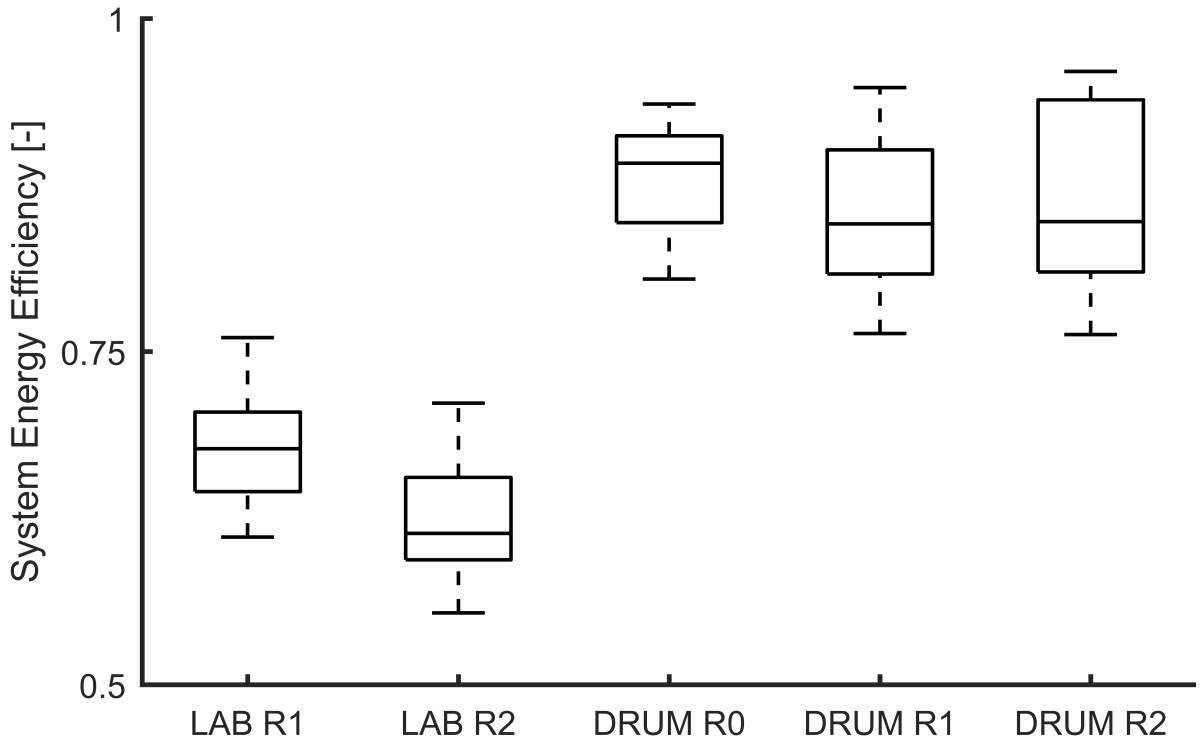

Fig. 5. Boxplots of the system energy efficiencies estimated over the middle of the columns when the smouldering front travelled between 0.3 to 0.5 m in the robust LAB and DRUM experiments.

The LAB system energy efficiency estimated here compares well with other laboratory estimates of radial heat losses from smouldering columns [13, 14, 55], which provides confidence in this approach. In agreement with predictions from Zanoni et al., Fig. 4 reveals that the magnitude of radial heat losses increases over time as the cooling zone thickness grows [13]. At sufficiently late times in long columns, all system energy efficiencies in Fig. 5 would approach a steady-state condition when radial heat losses balance the energy released from smouldering. Here, like nearly all other applied smouldering experiments in the literature and all smouldering reactors used in practice (e.g., [3, 12, 45]), the energy balances are far from this late-time condition.

3.2. The Effects of Heat Losses on Weak Smouldering Systems

As articulated in the Introduction, while moderate heat losses do not significantly affect robust smouldering, in weak smouldering cases they may lead to extinction [43, 56]. It was therefore hypothesized that reducing the radial heat losses, here by increasing scale, could transform a NSS scenario into a SS scenario. Indeed, this is demonstrated in Fig. 6. Figures 6(a) and 6(b) show LAB W1 and W2, two NSS experiments experiencing extinction due to critically low GAC concentration (10 g_{GAC} kg_s^{-1}) and critically low air flux (1 cm s^{-1}), respectively. Note that the LAB column limits (LAB W3 using 15 g_{GAC} kg_s^{-1} at 5 cm s^{-1}, and LAB W4 using 20 g_{GAC} kg_s^{-1} at 2 cm s^{-1} were SS, see Table 1) are consistent with applied smouldering literature, with minimum air fluxes around 0.5 – 1.4 cm s^{-1} [43, 88, 89] and minimum fuel mass fractions around 16 – 28 g_{fuel} kg_s^{-1} [29, 42, 43, 46]. Figures 6(c) and 6(d) show that DRUM W1 and W2, with the same experimental conditions as LAB W1 and W2, respectively, exhibited SS behaviour. This demonstrates that the reduced radial heat losses improved the global energy balance such that the smouldering behaviour shifted towards more robust conditions. These robust conditions meant that energy was generated faster than it was lost near the reactions, and quenching was avoided.

The ability for increasing scale to shift the extinction limits for smouldering to lower fuel concentrations and lower air flux values is confirmed by the mass loss curves for these four experiments (LAB W1 and W2, DRUM W1 and W2) in Fig. 2. This figure also reveals that, even though these two DRUM cases were SS, the fuel was not entirely oxidized. Though DRUM W1 fostered SS smouldering along the centre of the column, material near

the column walls experienced extinction as a wedge of unburned material increased in thickness with height but did not progress into the centre of the column (see a photo of the excavation in the Supplementary Materials, Fig S10). Therefore, DRUM W1 is qualified as borderline-self-sustaining, which was more robust than LAB W1 but would require further intervention to be fully self-sustaining. A rich discussion on various adjustments to improve smouldering robustness is presented in [13, 43]. However, it is also important to point out that the dynamics that lead to quenching in Fig. 6 are currently not well understood. Torero et al. discusses this knowledge gap and points out there is room for a harmonized explanation of extinction in smouldering systems [18].

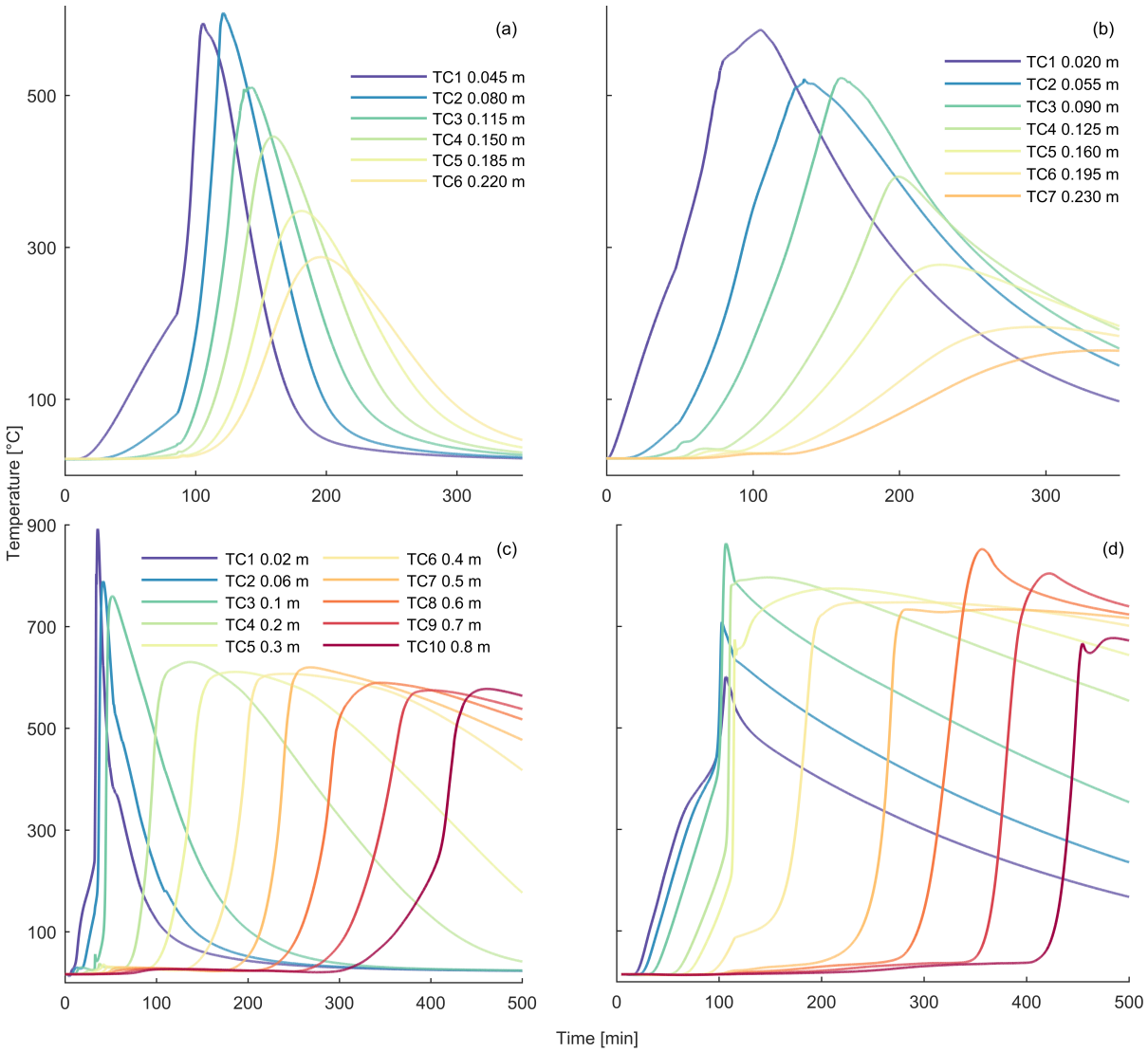

Fig. 6. Centreline temperature-time profiles showing: (a) Non-self-sustaining smouldering in the LAB due to critically low fuel concentration, LAB W1; (b) Non-self-sustaining smouldering in the LAB due to critically low air flux, LAB W2; (c) Borderline-Self-sustaining smouldering in the DRUM at low fuel concentration, DRUM W1; and (d) Self-sustaining smouldering in the DRUM at low air flux, DRUM W2, which had the same thermocouple layout as DRUM W1. All thermocouples were embedded in the fuel bed.

4. Summary and Conclusions

As the applications of smouldering combustion expand, in particular those related to waste-to-energy processes, there is a growing interest in designing systems to best house a propagating smouldering reaction. To effectively operate a smouldering system, it is necessary to determine the conditions that will result in the self-sustained propagation of the reaction. Radial heat losses have been demonstrated to play a major role on the stability of the smouldering reaction, therefore, understanding of the relationship between stability and reactor dimensions is critical. A novel approach to quantify the decreasing fraction of total energy lost radially from increasing the column radius has been presented and contrasted with experimental results and the impact of heat losses on the robustness of the reaction quantified. Through a global energy and mass balance, the impact of heat losses was normalized as the system energy efficiency by dividing the net stored energy from the energy added into the column for ignition and released from smouldering. This approach facilitated a valuable estimate of the system energy efficiency. The energy efficiency was found to increase with column radius from 65 ± 3% to 86 ± 5% in 0.080 m to 0.300 m radii columns, respectively. Weak smouldering experiments using low air fluxes and low fuel concentrations also showed that increased system energy efficiency increased the robustness of the reaction to quenching. Essentially, these results highlight how processes affecting global energy storage in the system, largely behind the forward smouldering front here, impact the local energy balance at the reaction zone under extreme conditions. Altogether, this work underscores the importance of scale as a

crucial design parameter in optimizing a smouldering system and provides a practical framework to estimate heat losses.

5. Acknowledgements

Funding was provided by the Ontario Ministry of Research, Innovation and Science; the Government of Canada through the Federal Economic Development Agency for Southern Ontario through the Ontario Water Consortium's Advancing Water Technologies Program (Grant SUB02392) with in-kind support from: 1) the Ontario Ministry of the Environment, Conservation and Parks and 2) Savron, a wholly owned subdivision of Geosyntec Consultants Ltd; and the Natural Sciences and Engineering Research Council of Canada (Graduate Scholarship PGSD3 - 489978 - 2016 and Grant Nos. CREATE 449311-14, RGPIN 2018-06464, and RGPAS-2018-522602). We gratefully acknowledge simulations performed by Dr. Marco Zanoni presented in the Supplementary Materials, GAC characterization performed by Jiahao Wang, and experiments LAB W1 and W4 performed by Joshua Brown, who all provided valuable input and assisted in subsequent experimental work, and additional project support from Gudgeon Thermfire International (particularly from Justin Barfett and Randy Adamski), Dr. Gavin Grant, Cody Murray, Taryn Fournie, Megan Green, Brendan Evers, Thomas Mathias, Dillon McIntyre, Jordan Teeple, Jad Choujaa, Maxwell Servos, Reid Clementino, Kia Barrow, Nick Rogowski, and Christopher Kwan.

6. References

[1] Grant GP, Major D, Scholes GC, Horst J, Hill S, Klemmer MR, et al. Smoldering Combustion (STAR) for the Treatment of Contaminated Soils: Examining Limitations and Defining Success. Rem J. 2016;26:27-51.

[2] Vidonish JE, Zygourakis K, Masiello CA, Sabadell G, Alvarez PJJ. Thermal Treatment of Hydrocarbon-Impacted Soils: A Review of Technology Innovation for Sustainable Remediation. Engineering. 2016;2:426-37.

[3] Sabadell G, Scholes G, Thomas D, Murray C, Bireta P, Grant G, et al. Ex situ treatment of organic wastes or oil-impacted soil using a smoldering process. WIT Trans Ecol Environ. 2019;231:367-76.

[4] Ronda A, Della Zassa M, Biasin A, Martin-Lara MA, Canu P. Experimental investigation on the smouldering of pine bark. Fuel. 2017;193:81-94.

[5] Gianfelice G, Della Zassa M, Biasin A, Canu P. Onset and propagation of smouldering in pine bark controlled by addition of inert solids. Renew Energ. 2019;132:596-614.

[6] Ronda A, Della Zassa M, Gianfelice G, Iáñez-Rodríguez I, Canu P. Smouldering of different dry sewage sludges and residual reactivity of their intermediates. Fuel. 2019;247:148-59.

[7] Feng C, Cheng M, Gao X, Qiao Y, Xu M. Occurrence forms and leachability of inorganic species in ash residues from self-sustaining smouldering combustion of sewage sludge. Proc Combust Inst. 2020:, https://doi.org/10.1016/j.proci.2020.06.008.

[8] Wyn HK, Konarova M, Beltramini J, Perkins G, Yermán L. Self-sustaining smouldering combustion of waste: A review on applications, key parameters and potential resource recovery. Fuel Process Technol. 2020;205:106425.

[9] Vantelon J-P, Lodeho B, Pignoux S, Ellzey JL, Torero JL. Experimental observations on the thermal degradation of a porous bed of tires. Proc Combust Inst. 2005;30:2239-46.

[10] Yermán L. Self-sustaining Smouldering Combustion as a Waste Treatment Process. In: Kyprianidis KG, Skvaril J, editors. Developments in Combustion Technology. Rijeka: InTech; 2016. p. 143-66.

[11] Saberi S, Samiei K, Iwanek E, Vohra S, Farkhondehkavaki M, Cheng Y-L. Treatment of fecal matter by smoldering and catalytic oxidation. Journal of Water, Sanitation and Hygiene for Development. 2020;10:219–26.

[12] Sabadell G, Thomas D, Bireta P, Scholes G, Murray C, Boulay B, et al. Treatment of Oil-Impacted Soil and Oily Waste: Overview of Two Field Demonstration Projects. SPE International Conference and Exhibition on Health, Safety, Security, Environment, and Social Responsibility. Abu Dhabi, UAE: Society of Petroleum Engineers; 2018. p. SPE-190566-MS.

[13] Zanoni MAB, Torero JL, Gerhard JI. Determining the conditions that lead to self-sustained smouldering combustion by means of numerical modelling. Proc Combust Inst. 2019;37:4043-51.

[14] Pozzobon V, Baud G, Salvador S, Debenest G. Darcy Scale Modeling of Smoldering: Impact of Heat Loss. Combust Sci Technol. 2017;189:340-65.

[15] Lutsenko NA. Numerical model of two-dimensional heterogeneous combustion in porous media under natural convection or forced filtration. Combust Theor Model. 2018;22:359-77.

[16] Ohlemiller TJ. Modeling of smoldering combustion propagation. Prog Energ Combust. 1985;11:277-310.

[17] Williams FA. Combustion theory. second ed. Menlo Park, California: Addison-Wesley Publishing Company; 1985.

[18] Torero JL, Gerhard JI, Martins MF, Zanoni MAB, Rashwan TL, Brown JK. Processes defining smouldering combustion: Integrated review and synthesis. Prog Energ Combust. 2020;81:100869.

[19] Williams FA. Mechanisms of fire spread. Symp (Int) Combust. 1977;16:1281-94.

[20] Page SE, Siegert F, Rieley JO, Boehm H-DV, Jaya A, Limin S. The amount of carbon released from peat and forest fires in Indonesia during 1997. Nature. 2002;420:61-5.

[21] Shi B, Su H, Li J, Qi H, Zhou F, Torero JL, et al. Clean Power Generation from the Intractable Natural Coalfield Fires: Turn Harm into Benefit. Sci Rep. 2017;7:5302.

[22] Santoso MA, Huang X, Prat-Guitart N, Christensen E, Hu Y, Rein G. Smouldering fires and soils. In: Pereira P, Mataix-Solera J, Úbeda X, Rein G, Cerdà A, editors. Fire Effects on Soil Properties. Clayton, VIC: CSIRO Publishing; 2019. p. 203–16.

[23] Rein G. Smoldering Combustion. In: Hurley MJ, Gottuk DT, Hall Jr JR, Harada K, Kuligowski ED, Puchovsky M, et al., editors. SFPE Handbook of Fire Protection Engineering. New York, NY: Springer New York; 2016. p. 581-603.

[24] Drysdale D. Spontaneous Ignition within Solids and Smoldering Combustion. An Introduction to Fire Dynamics. third ed. Chichester: John Wiley & Sons, Ltd.; 2011. p. 317-48.

[25] Gerhard JI, Grant GP, Torero JL. Chapter 9 - Star: a uniquely sustainable in situ and ex situ remediation process. In: Hou D, editor. Sustainable Remediation of Contaminated Soil and Groundwater: Butterworth-Heinemann; 2020. p. 221-46.

[26] Rein G. Smouldering Fires and Natural Fuels. In: Belcher CM, editor. Fire Phenomena and the Earth System: John Wiley & Sons; 2013. p. 15-33.

[27] Moussa NA, Toong TY, Garris CA. Mechanism of smoldering of cellulosic materials. Symp (Int) Combust. 1977;16:1447-57.

[28] Scholes GC, Gerhard JI, Grant GP, Major DW, Vidumsky JE, Switzer C, et al. Smoldering Remediation of Coal-Tar-Contaminated Soil: Pilot Field Tests of STAR. Environ Sci Technol. 2015;49:14334-42.

[29] Pironi P, Switzer C, Gerhard JI, Rein G, Torero JL. Self-sustaining smoldering combustion for NAPL remediation: laboratory evaluation of process sensitivity to key parameters. Environ Sci Technol. 2011;45:2980-6.

[30] Rashwan TL, Gerhard JI, Grant GP. Application of self-sustaining smouldering combustion for the destruction of wastewater biosolids. Waste Manage. 2016;50:201-12.

[31] Serrano A, Wyn H, Dupont L, Villa-Gomez DK, Yermán L. Self-sustaining treatment as a novel alternative for the stabilization of anaerobic digestate. J Environ Manage. 2020;264:110544.

[32] Howell J, Hall M, Ellzey J. Combustion of hydrocarbon fuels within porous inert media. Prog Energ Combust. 1996;22:121-45.

[33] Mujeebu MA, Abdullah MZ, Bakar MZA, Mohamad AA, Abdullah MK. Applications of porous media combustion technology – A review. Appl Energy. 2009;86:1365-75.

[34] Ellzey JL, Belmont EL, Smith CH. Heat recirculating reactors: Fundamental research and applications. Prog Energ Combust. 2019;72:32-58.

[35] Yermán L, Hadden RM, Carrascal J, Fabris I, Cormier D, Torero JL, et al. Smouldering combustion as a treatment technology for faeces: Exploring the parameter space. Fuel. 2015;147:108-16.

[36] Aldushin AP, Rumanov IE, Matkowsky BJ. Maximal energy accumulation in a superadiabatic filtration combustion wave. Combust Flame. 1999;118:76-90.

[37] Niessen WR. Combustion and incineration processes: applications in environmental engineering. third ed. New York, NY: Marcel Dekker, Inc.; 2002.

[38] Buekens A. Incineration Technologies. In: Meyers RA, editor. Encyclopedia of Sustainability Science and Technology. New York, NY: Springer New York; 2012. p. 5235-96.

[39] Makarichi L, Jutidamrongphan W, Techato K-a. The evolution of waste-to-energy incineration: A review. Renew Sust Energ Rev. 2018;91:812-21.

[40] Monhol FAF, Martins MF. Cocurrent Combustion of Human Feces and Polyethylene Waste. Waste Biomass Valorization. 2015;6:425-32.

[41] Pironi P, Switzer C, Rein G, Fuentes A, Gerhard JI, Torero JL. Small-scale forward smouldering experiments for remediation of coal tar in inert media. Proc Combust Inst. 2009;32:1957-64.

[42] Switzer C, Pironi P, Gerhard J, Rein G, Torero J. Self-sustaining smoldering combustion: a novel remediation process for non-aqueous-phase liquids in porous media. Environ Sci Technol. 2009;43:5871-7.

[43] Zanoni MAB, Torero JL, Gerhard JI. Delineating and explaining the limits of self-sustained smouldering combustion. Combust Flame. 2019;201:78-92.

[44] Switzer C, Pironi P, Gerhard JI, Rein G, Torero JL. Volumetric scale-up of smouldering remediation of contaminated materials. J Hazard Mater. 2014;268:51-60.

[45] Solinger R, Grant GP, Scholes GC, Murray C, Gerhard JI. STARx Hottpad for smoldering treatment of waste oil sludge: Proof of concept and sensitivity to key design parameters. Waste Manage Res. 2020;38:554-66.

[46] Baud G, Salvador S, Debenest G, Thovert J-F. New Granular Model Medium To Investigate Smoldering Fronts Propagation—Experiments. Energ Fuel. 2015;29:6780-92.

[47] Sennoune M, Salvador S, Quintard M. Toward the Control of the Smoldering Front in the Reaction-Trailing Mode in Oil Shale Semicoke Porous Media. Energ Fuel. 2012;26:3357-67.

[48] Yermán L, Wall H, Torero J, Gerhard JI, Cheng YL. Smoldering Combustion as a Treatment Technology for Feces: Sensitivity to Key Parameters. Combust Sci Technol. 2016;188:968-81.

[49] Yermán L, Wall H, Torero JL. Experimental investigation on the destruction rates of organic waste with high moisture content by means of self-sustained smoldering combustion. Proc Combust Inst. 2017;36:4419-26.

[50] Sennoune M, Salvador S, Quintard M. Reducing CO2 emissions from oil shale semicoke smoldering combustion by varying the carbonate and fixed carbon contents. Combust Flame. 2011;158:2272-82.

[51] Fadaei H, Sennoune M, Salvador S, Lapene A, Debenest G. Modelling of non-consolidated oil shale semi-coke forward combustion: Influence of carbon and calcium carbonate contents. Fuel. 2012;95:197-205.

[52] Kolesnikova YY, Kislov VM, Salgansky EA. Influence of the heat loss intensity on the characteristics of the filtration combustion of solid organic fuels. Russ J Phys Chem B. 2016;10:791-5.

[53] Wyn HK, Zárate S, Carrascal J, Yermán L. A Novel Approach to the Production of Biochar with Improved Fuel Characteristics from Biomass Waste. Waste Biomass Valorization. 2019.

[54] Salman M, Gerhard JI, Major DW, Pironi P, Hadden R. Remediation of trichloroethylene-contaminated soils by star technology using vegetable oil smoldering. J Hazard Mater. 2015;285:346-55.

[55] Martins MF, Salvador S, Thovert JF, Debenest G. Co-current combustion of oil shale – Part 2: Structure of the combustion front. Fuel. 2010;89:133-43.

[56] Torero JL, Fernandez-Pello AC. Natural convection smolder of polyurethane foam, upward propagation. Fire Saf J. 1995;24:35-52.

[57] Hadden R, Alkatib A, Rein G, Torero JL. Radiant Ignition of Polyurethane Foam: The Effect of Sample Size. Fire Technol. 2014;50:673-91.

[58] Yuan H, Restuccia F, Richter F, Rein G. A computational model to simulate self-heating ignition across scales, configurations, and coal origins. Fuel. 2019;236:1100-9.

[59] Restuccia F, Fernandez-Anez N, Rein G. Experimental measurement of particle size effects on the self-heating ignition of biomass piles: Homogeneous samples of dust and pellets. Fuel. 2019;256:115838.

[60] Della Zassa M, Ronda A, Gianfelice G, Zerlottin M, Canu P. Scale effects and mechanisms ruling the onset of wastewater sludges self-heating. Fuel. 2019;256:115876.

[61] Dosanjh SS, Pagni PJ, Fernandez-Pello AC. Forced cocurrent smoldering combustion. Combust Flame. 1987;68:131-42.

[62] Buckmaster J, Lozinski D. An elementary discussion of forward smoldering. Combust Flame. 1996;104:300-10.

[63] Ohlemiller TJ, Bellan J, Rogers F. A model of smoldering combustion applied to flexible polyurethane foams. Combust Flame. 1979;36:197-215.

[64] Akkutlu IY, Yortsos YC. The dynamics of in-situ combustion fronts in porous media. Combust Flame. 2003;134:229-47.

[65] Zanoni MAB, Torero JL, Gerhard JI. The role of local thermal non-equilibrium in modelling smouldering combustion of organic liquids. Proc Combust Inst. 2019;37:3109-17.

[66] Yang J, Chen H, Liu N. Heat Loss and Kinetic Effects on Extinction and Critical Self-Sustained Propagation of Forced Forward Smoldering. In: Harada K, Matsuyama K, Himoto K, Nakamura Y, Wakatsuki K, editors. Fire Science and Technology 2015: The Proceedings of 10th Asia-Oceania Symposium on Fire Science and Technology. Singapore: Springer Singapore; 2017. p. 831-40.

[67] Rein G, Carlos Fernandez-Pello A, Urban DL. Computational model of forward and opposed smoldering combustion in microgravity. Proc Combust Inst. 2007;31:2677-84.

[68] Rein G, Bar-Ilan A, Fernandez-Pello AC, Ellzey JL, Torero JL, Urban DL. Modeling of one-dimensional smoldering of polyurethane in microgravity conditions. Proc Combust Inst. 2005;30:2327-34.

[69] Dosanjh S, Pagni P. Forced countercurrent smoldering combustion. In: Marto PJ, Tanasawa I, editors. Proceedings of the 1987 ASME/JSME Thermal Engineering Joint Conference: American Society of Mechanical Engineers, New York; 1987. p. 165-73.

[70] Torero J, Fernandez-Pello A, Kitano M. Opposed forced flow smoldering of polyurethane foam. Combust Sci Technol. 1993;91:95-117.

[71] Bar-Ilan A, Rein G, Fernandez-Pello AC, Torero J, Urban D. Forced forward smoldering experiments in microgravity. Exp Therm Fluid Sci. 2004;28:743-51.

[72] Bar-Ilan A, Rein G, Walther DC, Fernandez-Pello∗ AC, Torero JL, Urban DL. The effect of buoyancy on opposed smoldering. Combust Sci Technol. 2004;176:2027-55.

[73] Walther DC, Fernandez-Pello AC, Urban DL. Space shuttle based microgravity smoldering combustion experiments. Combust Flame. 1999;116:398-414.

[74] Leach SV, Ellzey JL, Ezekoye OA. Convection, pyrolysis, and Damköhler number effects on extinction of reverse smoldering combustion. Symp (Int) Combust. 1998;27:2873-80.

[75] Liñán A. The asymptotic structure of counterflow diffusion flames for large activation energies. Acta Astronaut. 1974;1:1007-39.

[76] Williams FA. Progress in knowledge of flamelet structure and extinction. Prog Energ Combust. 2000;26:657-82.

[77] Huang X, Gao J. A review of near-limit opposed fire spread. Fire Saf J. 2020:103141.

[78] Yamazaki T, Matsuoka T, Nakamura Y. Near-extinction behavior of smoldering combustion under highly vacuumed environment. Proc Combust Inst. 2019;37:4083-90.

[79] Zanoni MAB, Torero JL, Gerhard JI. Experimental and numerical investigation of weak, self-sustained conditions in engineered smouldering combustion. Combust Flame. 2020;222:27-35.

[80] Duchesne AL, Brown JK, Patch DJ, Major D, Weber KP, Gerhard JI. Remediation of PFAS-Contaminated Soil and Granular Activated Carbon by Smoldering Combustion. Environ Sci Technol. 2020.

[81] Glassman I, Yetter RA. Combustion. fourth ed. London, UK: Academic Press; 2008.

[82] Kinsman L, Torero JL, Gerhard JI. Organic liquid mobility induced by smoldering remediation. J Hazard Mater. 2017;325:101-12.

[83] Sennoune M, Salvador S, Debenest G. Impact of a CO2-Enriched Gas on the Decarbonation of CaCO3 and the Oxidation of Carbon in the Smoldering Process of Oil Shale Semicoke. Energ Fuel. 2012;26:391-9.

[84] Martins MF, Salvador S, Thovert JF, Debenest G. Co-current combustion of oil shale – Part 1: Characterization of the solid and gaseous products. Fuel. 2010;89:144-51.

[85] Bergman TL, Lavine AS, Incropera FP, DeWitt DP. Fundamentals of Heat and Mass Transfer. seventh ed. New York, NY: John Wiley & Sons; 2011.

[86] Zanoni MAB, Torero JL, Gerhard JI. Determination of the interfacial heat transfer coefficient between forced air and sand at Reynold's numbers relevant to smouldering combustion. Int J Heat Mass Transfer. 2017;114:90-104.

[87] Gibbons JD, Chakraborti S. Nonparametric Statistical Inference: Revised and Expanded. fourth ed. New York, NY: Marcel Dekker, Inc.; 2003.

[88] MacPhee SL, Gerhard JI, Rein G. A novel method for simulating smoldering propagation and its application to STAR (Self-sustaining Treatment for Active Remediation). Environ Modell Softw. 2012;31:84-98.

[89] Hasan T, Gerhard JI, Hadden R, Rein G. Self-sustaining smouldering combustion of coal tar for the remediation of contaminated sand: Two-dimensional experiments and computational simulations. Fuel. 2015;150:288-97.